High-strength, High-toughness Aligned Polymer-based Nanocomposite Reinforced with Ultra-low Weight Fraction of Functionalized Nanocellulose

*Shiyu Geng,[1,3] Kun Yao,[2,3] Qi Zhou[2,3] and Kristiina Oksman[1,4]**

[1]Division of Materials Science, Department of Engineering Sciences and Mathematics, Luleå University of Technology, SE-971 87, Luleå, Sweden

[2]Division of Glycoscience, Department of Chemistry, KTH Royal Institute of Technology, AlbaNova University Centre, SE-106 91, Stockholm, Sweden

[3]Wallenberg Wood Science Center, Department of Fiber and Polymer Technology, KTH Royal Institute of Technology, SE-100 44 Stockholm, Sweden

[4]Fibre and Particle Engineering, University of Oulu, FI-90014, Oulu, Finland

ABSTRACT. Multifunctional lightweight, flexible, yet strong polymer-based nanocomposites are highly desired for specific applications. However, the control of orientation and dispersion of reinforcing nanoparticles and the optimization of the interfacial interaction still pose substantial challenges in nanocellulose-reinforced polymer composites. In this study, poly(ethylene glycol) (PEG)-grafted cellulose nanofibers has demonstrated much better dispersion in a poly(lactic acid) (PLA) matrix as compared with unmodified nanocellulose. Through a uniaxial drawing method,

aligned PLA/nanocellulose nanocomposites with high strength, high toughness, and unique optical behavior can be obtained. With the incorporation of 0.1 wt% of the PEG-grafted cellulose nanofibers in PLA, the ultimate strength of the aligned nanocomposite reaches 343 MPa, which is significantly higher than that of other aligned PLA-based nanocomposites reported previously. Moreover, its ultimate strength and toughness are enhanced by 39% and 70%, respectively, compared with the aligned nanocomposite reinforced with unmodified cellulose nanofibers. In addition, the aligned nanocomposite film is highly transparent and possesses an anisotropic light scattering effect, revealing its significant potential for optical applications.

KEYWORDS: nanocellulose, nanocomposite, alignment, mechanical characteristics, light scattering

INTRODUCTION

Polymer-based nanocomposites have recently attracted significant attention, because the combinations of properties of various polymers and nanomaterials used in these nanocomposites allow them to be designed and tailored for specific applications.[1-3] Nanocellulose with high stiffness and strength, large surface area, and biodegradability are promising as reinforcements in biodegradable polymer matrices to produce environment-friendly nanocomposites as replacements for fossil-based materials.[4] Cellulose nanofibers (CNFs) were first extracted by Turbak *et al*. in 1983,[5] and used as a reinforcing phase in polypropylene, high-density polyethylene, and polystyrene as reported by Boldizar *et al*. in 1987.[6] In 1995, Favier *et al*. first studied the reinforcing effect of cellulose nanocrystals (CNCs) on the mechanical properties of poly (styrene-co-butyl acrylate)-based nanocomposites.[7] Subsequently, CNF- or CNC-reinforced nanocomposites with different biodegradable polymer matrices, such as starch,[8-10] silk protein,[11-

[12] chitosan,[13-14] polyhydroxybutyrate,[15-16] poly(vinyl alcohol) (PVA),[17-19] and poly(lactic acid) (PLA),[20-23] have been investigated. More recently, Isogai *et al.* developed a new type of CNF with very fine diameters (3–4 nm) and large aspect ratios (>100) using 2,2,6,6-tetramethyl-piperidine-1-oxyl radical (TEMPO)-mediated oxidation,[24-25] abbreviated to TOCNF, which has considerable potential for use in many high-tech fields. In addition to strengthening the mechanical properties of the polymer composites,[26-28] TOCNF can also reduce the oxygen permeability of PLA films drastically while maintaining the transparency of the film,[29] which is favorable for packaging applications.

To overcome the problem of poor dispersion of nanocellulose materials in a hydrophobic polymer matrix, surface functionalization of nanocellulose has been performed and investigated.[30-32] The grafting of polymer brushes to nanocellulose using either a "grafting to" or "grafting from" approach is an important method to improve the dispersion of nanocellulose and the interaction between the nanocellulose and polymer matrix.[33] TOCNF is superior to native nanocellulose for selective and dense grafting of polymer owing to the carboxyl groups on its surface.[34-35] Grafting poly(ethylene glycol) (PEG) to TOCNF was first reported by Fujisawa *et al.*,[26,28] and it leads to a nano-dispersion state of the PEG-grafted TOCNFs in the PLA matrix, resulting in improvements of mechanical properties compared with those of neat PLA and carbon nanotube (CNT)-reinforced PLA composites. Tang *et al*. investigated oriented PEG-grafted TOCNF ribbons,[36] and observed that an elastic modulus of 32.3 GPa, strength of 576 MPa, and interesting light scattering behavior can be achieved.

To obtain unique anisotropic properties, drawing or stretching has been used to obtain aligned materials in polymers and polymer-based composites during the last few decades.[36-39] Drawing of PLA has attracted considerable attention because it not only enhances the elastic modulus and

ultimate strength of the PLA, but also significantly improves the elongation at break, which results in much higher toughness compared with that of isotropic PLA material.[40-42] However, only a few studies have investigated aligned PLA-based nanocomposites. Tabatabaei *et al.* studied the uniaxial and biaxial stretched PLA/nanoclay composite films, and observed that the silicate layers in nanoclays were aligned in the flow direction in the uniaxial stretched films and the crystallite unit cells of PLA were more oriented owing to the incorporation of nanoclays.[43] Blaker *et al.* produced aligned PLA/nanocellulose composite fibers by melt-spinning, and further developed a method similar to layered filament winding to produce bulky composites that retain the aligned fiber structure.[44] Mai *et al.* confirmed that a high degree of alignment of CNTs was achieved in the oriented PLA/CNT composite tapes, and the reinforcing efficiency of CNT was enhanced owing to the alignment, resulting in a tensile strength of 156 MPa of the oriented composite with 2 wt% CNT at a draw ratio of 7.5.[45]

In our previous work,[46] aligned nanocomposites consisting of plasticized PLA and 1 wt% of CNF were obtained via liquid-assisted extrusion followed by solid-state drawing. We investigated the effects of draw ratio, temperature, and speed on the properties of the nanocomposites, and determined that the strength and toughness of the nanocomposite drawn at 40 °C with a speed of 100 mm/min and a draw ratio of 2.5 reached 102 MPa and 70 MJ/m^3, respectively, which were 2 and 47 times higher than those of the undrawn sample. Inspired by the previous studies on PEG-grafted TOCNF and drawing of PLA,[26-28,36,40-46] and with the consideration of the relatively high energy consumption in the production of nanomaterials,[47-48] herein, we present an aligned PLA-based nanocomposite reinforced with only 0.1 wt% of PEG-grafted TOCNF, which demonstrates high strength, high toughness, and unique optical properties. The structure of the nanocomposites before and after drawing was examined using various microscopy techniques. Moreover, the

effects of grafting PEG to TOCNF on structure and properties of the aligned PLA/TOCNF nanocomposites are investigated and discussed, as compared to unmodified TOCNF reinforced-PLA and the nanocomposites containing free PEG.

EXPERIMENTAL SECTION

Materials. The preparation of TOCNF and PEG-grafted TOCNF (TOCNF-*g*-PEG) was described by Tang *et al*.[36] Briefly, a never-dried softwood pulp was treated via TEMPO-mediated oxidation to generate carboxylated pulp fibers. To prepare native TOCNFs, the carboxylated pulp fibers were mechanical disintegrated directly to generate an aqueous TOCNF suspension (0.45 wt%). To prepare TOCNF-*g*-PEG, the carboxylated pulp fibers were functionalized via carbodiimide-mediated amidation with PEG-NH_2 (M_n = 750) followed by mechanical disintegration to achieve an aqueous TOCNF-*g*-PEG suspension (0.6 wt% of solid content). PLA (Ingeo 4032D) was purchased from NatureWorks, Nebraska, USA. Hydrochloric acid, sodium hydroxide, *N,N*-dimethylformamide (DMF, anhydrous) and methoxy-PEG (M_n = 750) were purchased from Sigma–Aldrich, St Louis, USA. All chemicals were used as received.

Preparation of isotropic and aligned nanocomposites. A certain amount of the TOCNF or TOCNF-*g*-PEG suspension was dispersed in DMF at first and thereafter, the PLA pellets were added. The suspension (5 wt% of solid content) was continuously stirred at 80 °C until the PLA pellets were completely dissolved, and thereafter, it was poured into a Teflon petri dish and dried in an oven with a fan at 80 °C for 24 h. The dried film was peeled off and compression-molded using a LabEcon 300 laboratory press (Fontijne Grotnes, Netherlands) at 190 °C under a pressure of 2.2 MPa for 1 min with 2 min of pre-heating to obtain the final isotropic nanocomposite reinforced by TOCNFs or TOCNF-*g*-PEG. The nanocomposite containing TOCNFs and free PEG was prepared using a similar process but with the addition of methoxy-PEG in DMF (the same

amount as the grafted PEG). The compositions of all the prepared isotropic nanocomposites and their sample codes can be seen in Table 1. To prepare the aligned nanocomposite, the isotropic film was drawn using a Shimadzu AG-X universal testing machine (Kyoto, Japan) at 100 °C in a Shimadzu THC1-200SP thermostatic chamber with a draw speed of 100 mm·min^{-1} and a draw ratio of 8. After drawing, the film was rapidly cooled down to room temperature (approximately 20 °C) and the aligned film was obtained. The isotropic and aligned neat PLA films were prepared in a similar manner as the nanocomposites.

Table 1. The compositions of all the isotropic samples prepared in this study.

Sample coding	Reinforcement (and additive)	PLA content (wt%)	TOCNF content (wt%)	PEG content* (wt%)
PLA	N/A	100.00	0.00	0.00
P0.1TOCNF	TOCNF	99.90	0.10	0.00
P0.1TOCNF-*g*-PEG	TOCNF-*g*-PEG	99.85	0.10	0.05
P0.1TOCNF/PEG	TOCNF/free PEG	99.85	0.10	0.05

*The grafted PEG content in TOCNF-*g*-PEG was determined by thermogravimetric analysis. Details are shown in the following Results and Discussion part.

Characterizations. The grafting of PEG on TOCNF was confirmed through Fourier-transform infrared spectroscopy (FTIR) with a Perkin-Elmer Spectrum 2000 FTIR spectrometer equipped with an attenuated total reflectance system and an MKII Golden Gate (Specac Ltd., London, UK). The samples were freeze dried and thereafter scanned in a spectral range of 600–4000 cm^{-1} with a resolution of 4 cm^{-1}. The content of grafted PEG was measured using thermogravimetric analysis (TGA) with a Mettler Toledo TGA/DSC 1STA Re System in nitrogen atmosphere. The samples were heated from 30 °C to 700 °C at a heating rate of 10 °C·min^{-1}. The

carboxylate content of TOCNF and TOCNF-*g*-PEG was determined by conductometric titration. Typically, the pH of a certain amount of the suspension was adjusted to 3 with hydrochloric acid (0.01 M), and thereafter the suspension was titrated with standardized sodium hydroxide solution (0.05 M) to reach a pH of 11. At the same time, the conductivity was monitored by a conductometric station (SevenCompact, Mettler-Toledo, USA). The morphology of TOCNF and TOCNF-*g*-PEG was investigated using atomic force microscopy (AFM) and transmission electron microscopy (TEM). For AFM, the samples were diluted to 0.001 wt% of solid content and deposited on freshly cleaved mica, and thereafter scanned using a Veeco MultiMode scanning probe (Santa Barbara, USA) with Bruker TESPA tips in AFM tapping mode. The same AFM setup was also used to investigate the unetched and etched surfaces of aligned P0.1TOCNF-*g*-PEG to obtain the 3D topography images. For TEM, the samples were deposited on a carbon-coated grid and treated with 1% uranyl acetate negative stain, and thereafter observed using a Hitachi Model HT7700 TEM (Tokyo, Japan) in high-contrast mode at 100 kV. The thermal behaviors of the isotropic and aligned samples were examined by differential scanning calorimetry (DSC) using a Mettler Toledo DSC 821^{e} from −20 °C to 220 °C at a scanning rate of 10 °C·min^{-1} in nitrogen atmosphere. The cross-sections and surfaces of the isotropic and aligned films were studied by scanning electron microscopy (SEM) using an FEI Magellan 400 XHR-SEM (Hillsboro, USA) with tungsten coating (Bal-Tec MED 020 coating system). The birefringence behaviors of the aligned samples were observed using a Nikon Eclipse LV100 POL polarized optical microscope (POM, Kanagawa, Japan). The mechanical properties of the isotropic and aligned samples were measured using the Shimadzu AG-X universal testing machine in tensile mode with an SLBL-1kN load cell. The isotropic samples were tested with a gauge length of 30 mm and crosshead speed of 5 mm·min^{-1}. The aligned samples were tested with a gauge length of 10 mm and crosshead speed

of 1 mm·min^{-1}. All the samples were conditioned at 20 °C and 6% humidity during the testing using the Shimadzu THC1-200SP thermostatic chamber to avoid the influence of moisture. The toughness of the samples was determined as work of fracture from the stress-strain curves. The light transmittance of the aligned P0.1TOCNF-*g*-PEG was measured using a Perkin Elmer UV-vis Spectrometer Lambda 2S (Überlingen, Germany) from 200 nm to 800 nm with a scan speed of 240 mm·min^{-1}. The light scattering behaviors of the samples were tested with a 635-nm laser source, and the distance between the laser source and sample was approximately 5 cm and that between the sample and detector was approximately 20 cm. The crystal structure of PLA in the isotropic and aligned samples was examined by X-ray diffraction (XRD) using an Empyrean X-ray diffractometer (PANalytical, UK) with CuKα radiation (λ = 1.5418 Å) in a 2θ angular range of 5–40° at a scan speed of 0.01 °·s^{-1}.

RESULTS AND DISCUSSION

The chemical structures of the native TOCNF and TOCNF-*g*-PEG prepared in this study are schematically illustrated in Figure 1a. The successful grafting of amine-terminated PEG to TOCNFs was confirmed using FTIR as shown in Figure 1b. The intensity of the bands at 1459 cm^{-1} and 2894 cm^{-1} in the spectrum of the TOCNF-*g*-PEG, corresponding to the CH_2 bending and stretching, respectively,[49-50] was significantly higher than that of the TOCNF, which is attributed to the grafting of PEG chains. Moreover, the intensity of the band representing the C=O stretching in carboxylate anions at 1600 cm^{-1} in the TOCNF-*g*-PEG spectrum decreased significantly compared with that in the TOCNF spectrum,[51] owing to the amide bond formation between the carboxyl groups of TOCNF and the amine groups from PEG-NH_2.

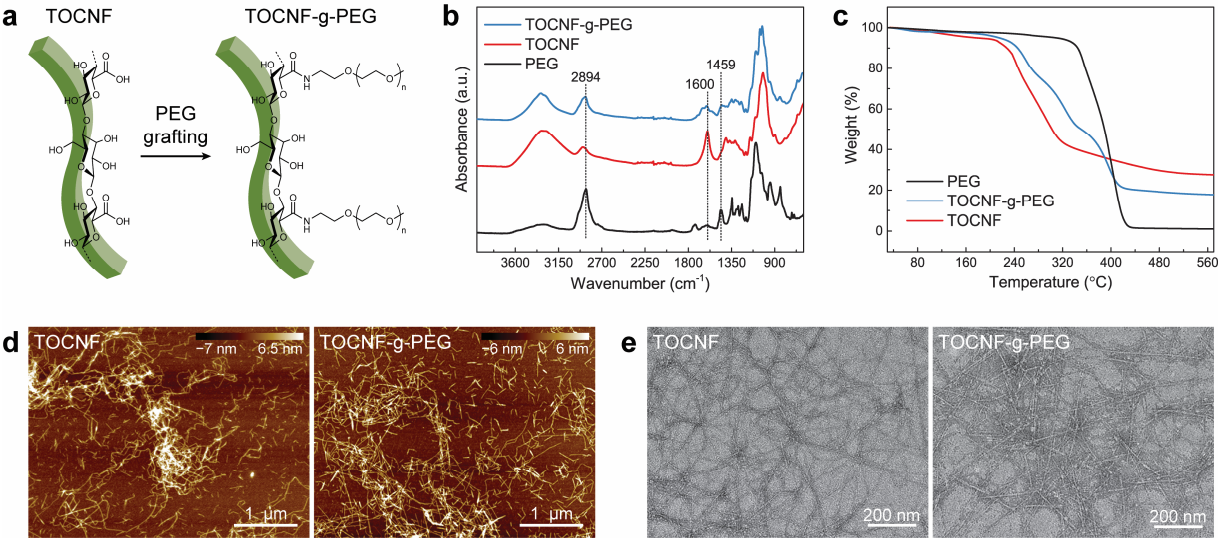

Figure 1. (a) Schematic illustration of the chemical structures of TOCNF and TOCNF-*g*-PEG. (b) FTIR spectra of PEG, TOCNF, and TOCNF-*g*-PEG. (c) TGA curves of PEG, TOCNF, and TOCNF-*g*-PEG. (d) AFM height images of TOCNF and TOCNF-*g*-PEG. (e) TEM images of TOCNF and TOCNF-*g*-PEG.

The amount of grafted PEG in the TOCNF-*g*-PEG was estimated from the inflexion points in the TGA curves (Figure 1c) according to the method described by Tang *et al.*[36] By extrapolating the onset of the degradation of PEG (approximately 340 °C) and the charring process of the residue (approximately 415 °C) in the curve of TOCNF-*g*-PEG, the grafting amount of PEG was determined as 31 wt%. Moreover, Figure 1c shows that the TOCNF-*g*-PEG has higher thermal stability than the native TOCNF since its degradation onset shifted to a higher temperature. This is because the layer of the grafted PEG surrounding the TOCNF acted as a shield during the heating process. According to the conductometric titration results shown in Figure S1 (Supporting Information), the carboxylate content of TOCNF and TOCNF-*g*-PEG are 1.2 mmol·g^{-1} and 0.43 mmol·g^{-1}, respectively. Thus, the degree of substitution of grafted PEG for carboxylate groups was calculated as 0.64 (Equation S1, Supporting Information). Both AFM and TEM images (Figure 1d,e) reveal that the morphologies of the TOCNF and TOCNF-*g*-PEG are similar, and their size

distribution histograms measured according to the TEM images are shown in Figure S2 (Supporting Information). The average width of the TOCNF-*g*-PEG is 4.3 nm, which is slightly larger than that of the TOCNFs (3.6 nm) owing to the grafted PEG layer covering the surface of the TOCNFs. The theoretical thickness of the grafted PEG layer in its good solvent was calculated according to Equation S2–S6 (Supporting Information),[26,52-53] which is equal to 3 nm. There is no apparent difference between the average lengths of the TOCNF (820 nm) and TOCNF-*g*-PEG (830 nm), indicating that the treatment of PEG grafting was mild and no degradation of the TOCNF occurred.

To investigate the effects of grafting PEG to TOCNF and drawing process on both the structure and properties of the PLA-based nanocomposites, samples reinforced with native TOCNFs, TOCNF-*g*-PEG, as well as TOCNFs with free PEG were prepared in this study. The TOCNF content in all the samples is 0.1 wt%, as shown in Table 1. Figure 2a illustrates that the isotropic samples were produced using solvent casting method followed by compression molding, and thereafter drawn at 100 °C with a draw ratio of 8 to obtain the aligned nanocomposites. The drawing temperature was determined according to the DSC thermograms of the isotropic samples (the thermal parameters are listed in Table S1, Supporting Information), which is expected to be between the glass transition temperature (T_g) and cold crystallization temperature (T_{cc}), but closer to T_{cc}. The obtained transparent isotropic and aligned nanocomposite films are illustrated in Figure 2b and c, respectively.

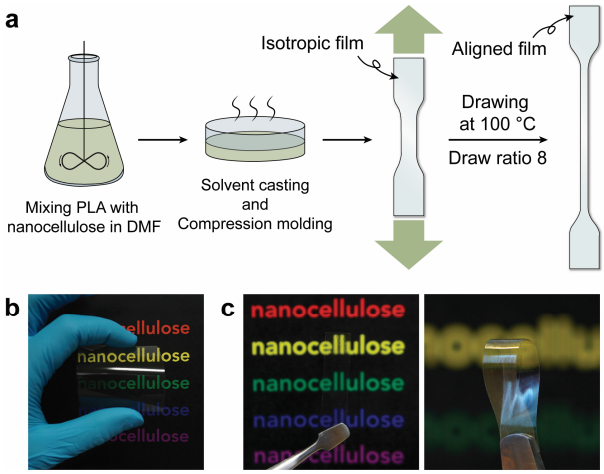

Figure 2. (a) Schematic illustration of the preparation process for the aligned nanocomposite films, and photographs of the (b) isotropic and (c) aligned P0.1TOCNF-*g*-PEG films.

The fracture surfaces of the isotropic samples were examined using SEM and the images are shown in Figure 3. Compared with the neat PLA, large TOCNF agglomerates can be observed in the P0.1TOCNF, which are attributed to the van der Waals forces and hydrogen bonds between the TOCNFs and the incompatibility between the hydrophilic TOCNF and hydrophobic PLA.[1] Owing to the addition of free PEG to the composite, the P0.1TOCNF/PEG shows much fewer TOCNF aggregates and a more ductile fracture surface. Furthermore, no TOCNF aggregates are observed in the P0.1TOCNF-*g*-PEG, which is due to the improved compatibility between TOCNF and PLA and the steric effect provided by the grafted PEG.[26,28,34] The SEM results indicate that both free and grafted PEG improve the dispersion of TOCNF in the PLA matrix, and grafting PEG to TOCNF is more efficient to achieve a homogenous structure in the nanocomposite.

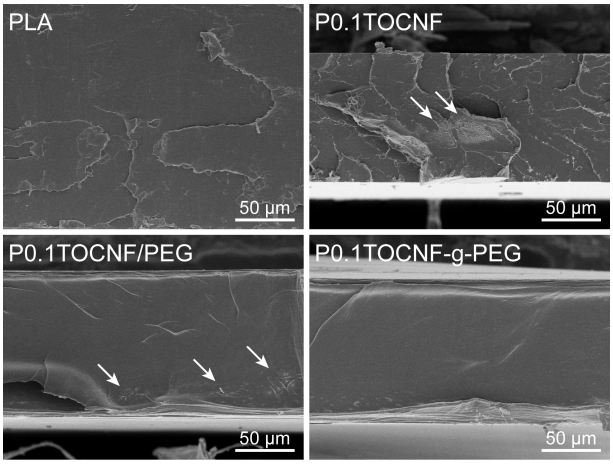

Figure 3. SEM images of the fracture surfaces of isotropic neat PLA, P0.1TOCNF, P0.1TOCNF/PEG and P0.1TOCNF-*g*-PEG films. Aggregates are indicated by white arrows.

After drawing, all the aligned materials exhibit extraordinary birefringence at an angle of 45° to the directions of the crossed polarizers under a POM as shown in Figure 4, while negligible light transmittance was demonstrated at the angle of 0° (Figure S3, Supporting Information). This indicates that high degrees of alignment of the polymer chains were achieved for all the materials by drawing.[54] However, the aligned neat PLA exhibits heterogeneous orientation from the center to the edge of the film, resulting from the relatively strong dipolar interaction among the PLA chains.[55] The aligned P0.1TOCNF shows an apparent disordered part in the center because large TOCNF agglomerates hinder the alignment of the PLA chains during the drawing process, which corresponds to the SEM result of the isotropic film (Figure 3). Both aligned P0.1TOCNF/PEG and P0.1TOCNF-*g*-PEG exhibit much more homogeneous alignment, which is attributed to the better dispersion of TOCNFs and the plasticizing effect of both free and grafted PEG, contributing to the movement of the PLA and TOCNFs in the nanocomposites.

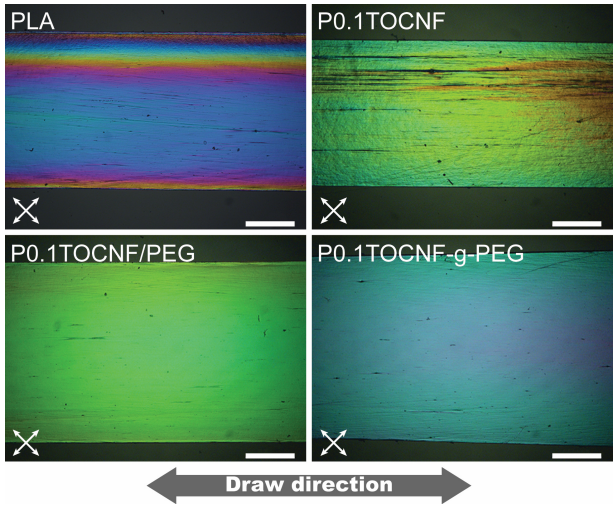

Figure 4. Polarized optical microscopy images of the surfaces of aligned neat PLA, P0.1TOCNF, P0.1TOCNF/PEG and P0.1TOCNF-*g*-PEG films (scale bar, 500 μm; directions of the crossed polarizers are shown in the lower left corner).

The surface structure of the aligned P0.1TOCNF-*g*-PEG was further characterized by SEM and AFM as shown in Figure 5. To observe the aligned structure more easily and investigate the PLA crystalline structure, etching was performed to the aligned sample and the etched surface was also examined. The unetched surface of the aligned P0.1TOCNF-*g*-PEG reveals small wrinkles parallel to the drawing direction as shown in Figure 5a. The formation of the wrinkles is due to the transverse compressive stress arising from the inability to accommodate the Poisson contraction of the sample near clamped edges.[56] The wrinkles are more obvious in the 3-dimensional (3D) AFM image illustrated in Figure 5c, and their average depth is measured as 5.3 ± 1.0 nm according to the topography section curve (Figure S4, Supporting Information). After being etched with an alkaline solution, the oriented structure in the aligned P0.1TOCNF-*g*-PEG became much more distinct as illustrated in Figure 5b,d and Figure S5 (Supporting Information), because part of the amorphous regions of PLA were etched out.[57] The magnified 3D AFM image in Figure 5e exhibits clearly that the periodic annular features present on the etched surface, which is attributed to the

PLA crystalline region in the aligned sample. Similar behaviors were reported in our previous work,[46] indicating that the "shish-kebab" crystalline structure was formed in the drawing process.

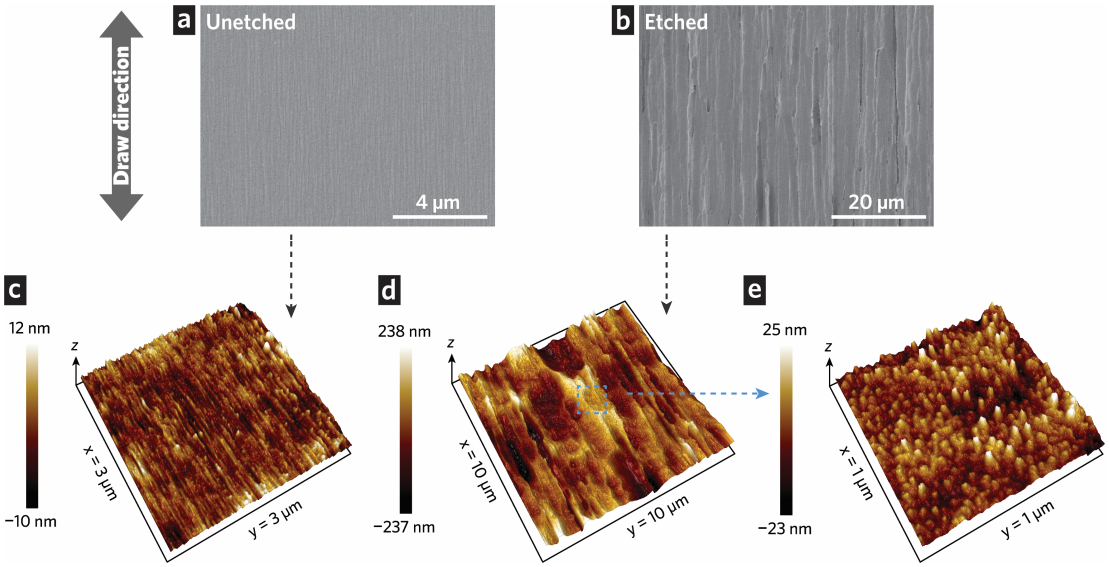

Figure 5. SEM images of (a) unetched and (b) etched surfaces of aligned P0.1TOCNF-*g*-PEG, and 3D AFM height images of the (c) unetched and (d,e) etched surfaces. The etched sample was obtained by etching the aligned film at 60 °C for 6 h in a 0.025M sodium hydroxide solution (with 1:2 water–methanol solvent).

To investigate the mechanical properties of the isotropic and aligned samples, tensile tests were conducted. The representative stress–strain curves of the aligned samples and isotropic P0.1TOCNF-*g*-PEG are shown in Figure 6a, and the mechanical properties of all the samples are summarized in Table S2 (Supporting Information). The drawing process provides a synergistic effect as the elastic modulus, ultimate strength, and elongation at break of all the samples are enhanced drastically. The improved elastic modulus and ultimate strength are attributed to the alignment of the PLA chains and TOCNFs, and the improved elongation at break is probably due to the "shish-kebab" structure formed during drawing, as demonstrated in Figure 5e. The inset photograph in Figure 6a indicates the fibrillation behavior of the aligned samples after break during

the tensile testing, which confirms that the highly aligned structure was introduced in the drawing process.

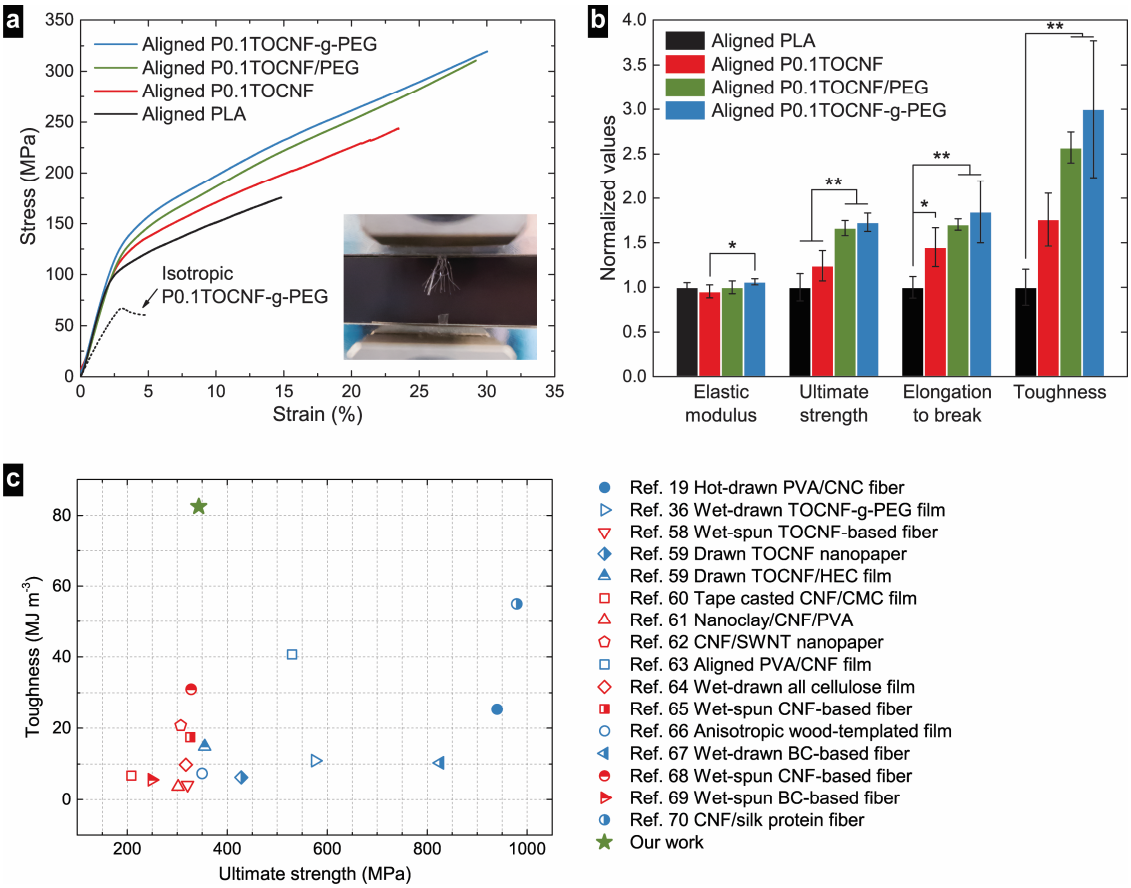

Figure 6. (a) Representative stress–strain curves of isotropic and aligned samples from tensile test. (b) Comparison of mechanical properties of aligned samples. All data were normalized according to the results of aligned neat PLA. ANOVA and Tukey-HSD comparison test was performed: *, $p < 0.05$; **, $p < 0.01$. (c) Toughness and ultimate strength of the aligned P0.1TOCNF-*g*-PEG compared with other anisotropic nanocellulose-based materials reported in the literature. Abbreviations: HEC, hydroxyethyl cellulose; CMC, carboxymethyl cellulose; SWNT, single-walled carbon nanotubes; BC, bacterial cellulose.

Figure 6b shows that the aligned P0.1TOCNF-*g*-PEG outperforms the other samples with respect to ultimate strength, elongation at break, and toughness. Compared with those of the aligned neat PLA, the ultimate strength and toughness of the aligned P0.1TOCNF-*g*-PEG are

improved by 73% and 200%, respectively, indicating that very high reinforcing efficiency can be achieved through the ultra-low weight fraction of well-dispersed TOCNF-*g*-PEG. The ultimate strength of the aligned P0.1TOCNF-*g*-PEG is as high as 343 MPa, which is significantly higher than that of the aligned PLA-based nanocomposites reported previously in literature.[41,44-46] Moreover, the ultimate strength and toughness of both aligned P0.1TOCNF/PEG and P0.1TOCNF-*g*-PEG are significantly higher than those of the aligned P0.1TOCNF, owing to the reduction of degree of aggregation of TOCNFs in PLA, corresponding to the microscope results shown in Figure 3 and 4. Compared with other studies on high-performance nanocellulose-based materials with anisotropic structure as shown in Figure 6c,[19,36,58-70] our aligned P0.1TOCNF-*g*-PEG exhibits competitive ultimate strength and superior toughness with only 0.1 wt% of nanocellulose, indicating a promising future of utilizing this kind of materials in low-cost and environment-friendly applications.

However, it needs to be noted that there is no significant difference in the elastic modulus of the aligned samples as illustrated in Figure 6b. This indicates that the elastic modulus of the aligned PLA-based nanocomposites with such a low fraction of reinforcement is mainly controlled by the alignment and crystallization of PLA chains. Furthermore, according to the ANOVA and Tukey-HSD comparison test, the difference in mechanical properties between the aligned P0.1TOCNF/PEG and P0.1TOCNF-*g*-PEG is not distinct since the p-value is greater than a significance level of 0.05. The possible reason is that the improvement of interaction between PLA and TOCNFs arising from the PEG grafting is limited, caused by the very thin layer of the grafted PEG (a theoretical thickness of 3 nm, Equation S6, Supporting information), and meanwhile the ultra-low weight fraction of the TOCNFs further reduces the impact of the improved interaction.

The effects of drawing process and TOCNF-*g*-PEG on the PLA-based nanocomposites are schematically illustrated in Figure 7. The undrawn semi-crystalline PLA as shown in Figure 7a consists of amorphous PLA chains and spherulites. During the drawing process at the temperature above T_g, the amorphous PLA chains are stretched and more orderly packed, and form a special crystalline structure like "shish-kebab" as shown in Figure 7b. This special crystal formation in aligned polymers was firstly reported by Pennings *et al*. in 1970.[71] The degree of crystallinity of PLA can be increased drastically due to drawing, which was confirmed through the DSC results in Table S1 (Supporting information). The aligned structure of PLA in the materials not only contributes to their strength and stiffness, but also improves elongation to break significantly (see Figure 6a). The reason is expected to be that the aligned PLA chains can slide between each other more easily compared to the disordered state with considerable entanglement effect in the isotropic materials.

In the case of aligned P0.1TOCNF demonstrated in Figure 7c, the appearance of TOCNF agglomerates influences the alignment of PLA chains and the crystalline structure, which was confirmed by the POM image in Figure 4. Consequently, it exhibits much lower strength and elongation to break than the aligned P0.1TOCNF-*g*-PEG as shown in Figure 6. Figure 7d shows that grafting PEG enhances the dispersion of TOCNFs in the PLA matrix, which further contributes to the better mechanical properties because the well-dispersed PEG-grafted TOCNFs provide higher reinforcing efficiency and bridging effect to the nanocomposite.

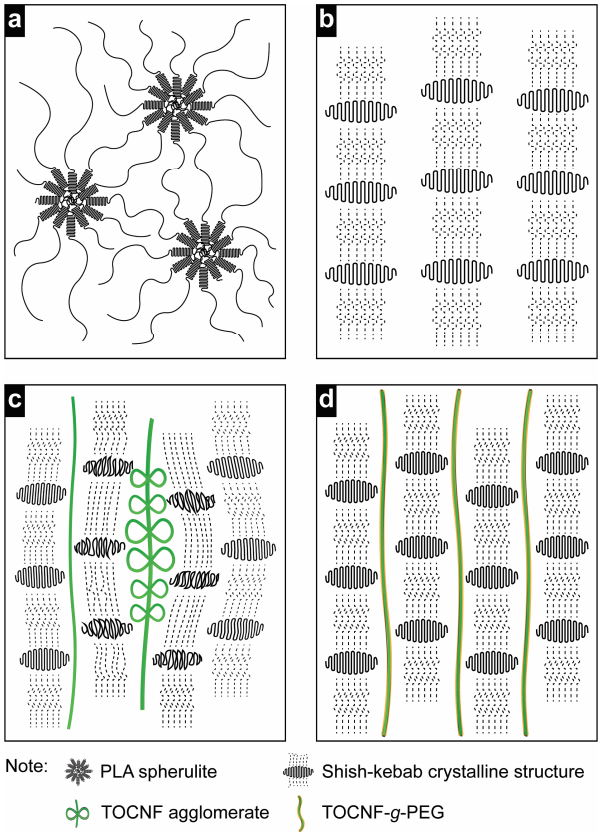

Figure 7. Schematic structures of (a) isotropic neat semi-crystalline PLA, (b) aligned neat PLA with "shish-kebab" crystalline structure, (c) aligned P0.1TOCNF with TOCNF agglomerates and (d) aligned P0.1TOCNF-*g*-PEG with well-dispersed PEG-grafted TOCNFs.

The optical properties of the aligned samples were also examined in this study. In addition to the birefringence behavior shown in Figure 4, the transparency of the aligned P0.1TOCNF-*g*-PEG was measured, which indicates a specular transmittance of more than 90% in a wavelength range of 350 to 800 nm as shown in Figure S6 (Supporting Information). The photograph in Figure 2c also demonstrates high transparency of the aligned nanocomposite film. Notably, the crystallinity of PLA in P0.1TOCNF-*g*-PEG is increased from 4.7% to 54.5% after drawing according to the DSC analysis (Table S1, Supporting Information), but the aligned sample is still transparent whereas annealed PLA films with high crystallinity are usually translucent.[72] A possible reason is

that the size of the PLA crystallites formed during the drawing process is much smaller than that generated during annealing treatment, which is confirmed using XRD analysis shown in Figure S7 (Supporting Information). The XRD scattering pattern of the aligned P0.1TOCNF-*g*-PEG exhibits a wider peak at $2\theta = 16.5°$ corresponding to (110)/(200) planes of PLA crystallites compared with that of the annealed isotropic sample, which indicates that smaller crystallites were obtained in the aligned sample according to the Scherrer equation (Equation S8, Supporting Information).[73]

Figure 8a illustrates the method employed for the light scattering test and the results are shown in Figure 8b. Compared with the isotropic P0.1TOCNF-*g*-PEG, the aligned film indicates obvious anisotropic light scattering behavior, which is attributed to its highly oriented structure as illustrated in the SEM and AFM images in Figure 5. The small wrinkles on the unetched surface of the sample could also contribute to the light scattering effect.[36] The light scattering behavior helps increase the light absorption and decrease the light reflection of the materials, resulting in improved performance of solar cells and display devices,[74-75] which indicates that the aligned P0.1TOCNF-*g*-PEG has significant potential for use in optical applications.

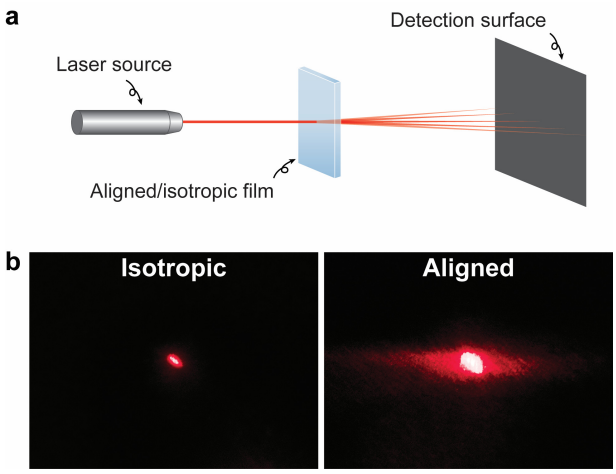

Figure 8. (a) Schematic illustration of light scattering test and (b) light scattering patterns after the laser passes through isotropic and aligned P0.1TOCNF-*g*-PEG.

CONCLUSIONS

In conclusion, grafting PEG to TOCNF affords better dispersion of TOCNFs in the PLA matrix compared with the unmodified TOCNF, thereby resulting in more homogenous alignment of the nanocomposite after uniaxial drawing, which contributes to superior mechanical properties and unique optical behaviors at an exceptionally low loading. Compared with that of the aligned PLA and P0.1TOCNF, the toughness of the aligned P0.1TOCNF-*g*-PEG exhibits 200% and 70% enhancement, respectively. The addition of free PEG in the unmodified TOCNF-reinforced PLA nanocomposite also improves the dispersion of the TOCNFs, but it is less efficient than that of grafted PEG because better interaction between TOCNF and PLA can be introduced through the covalent grafting process. The aligned P0.1TOCNF-*g*-PEG is not only strong and highly transparent but also has an anisotropic light scattering effect, indicating its excellent potential for use in optical applications such as solar cells and displays. Compared with other inspiring studies on nanocomposites with large loadings of nanomaterials,[19,36,58-70] we demonstrate the possibility of producing low-cost functional nanocomposites with competitive properties realized using an ultra-low amount of functionalized nanocellulose (0.1 wt% of total composite weight) and a drawing process, which facilitates their usage in large-scale applications. More importantly, both PLA and nanocellulose are biopolymers which are derived from renewable resources and biodegradable, indicating that the aligned nanocomposites consisting of them are environmentally friendly and highly desired for the sustainable development.

ASSOCIATED CONTENT

Supporting information

Conductometric titration of TOCNF and TOCNF-*g*-PEG. Size distributions of TOCNF and TOCNF-*g*-PEG. Calculation of degree of substitution of grafted PEG to carboxylate groups. Calculation of average density of grafted PEG on TOCNF-*g*-PEG. Calculation of thickness of grafted PEG layer. DSC thermal parameters of all the samples. POM image of aligned P0.1TOCNF-*g*-PEG (0° to the crossed polarizers). Topography section curve of the unetched surface of the aligned P0.1TOCNF-*g*-PEG. An additional SEM image of aligned P0.1TOCNF-*g*-PEG after etching. Mechanical properties of all the samples. Light transmittance of aligned P0.1TOCNF-*g*-PEG. XRD scattering patterns of isotropic and aligned P0.1TOCNF-*g*-PEG. Scherrer equation.

AUTHOR INFORMATION

Corresponding Author

*E-mail: kristiina.oksman@ltu.se

Notes

The authors declare no competing financial interest.

ACKNOWLEDGMENTS

The authors thank Dr. Anshu Anjali Singh for the valuable discussions, Dr. Natalia Herrera for the technical support regarding light transmittance test, M.Sc. Hanzhu Zhang for the technical support regarding XRD, Maria Harila for the assistance in sample preparation, and the financial support from Knut och Alice Wallenberg Stiftelsen, TEKES FiDiPro Programme, Bio4Energy, SNS WOOD-PRO and Kempe Foundation.

REFERENCES

1. Ajayan, P. M.; Schadler, L. S.; Braun, P. V., *Nanocomposite science and technology*. John Wiley & Sons: 2006.
2. Paul, D.; Robeson, L. M., Polymer nanotechnology: nanocomposites. *Polymer* **2008,** *49* (15), 3187-3204.
3. Lee, K.-Y.; Aitomäki, Y.; Berglund, L. A.; Oksman, K.; Bismarck, A., On the use of nanocellulose as reinforcement in polymer matrix composites. *Compos. Sci. Technol.* **2014,** *105*, 15-27.
4. Dufresne, A., *Nanocellulose: from nature to high performance tailored materials*. Walter de Gruyter: 2013.
5. Turbak, A. F.; Snyder, F. W.; Sandberg, K. R. In *Microfibrillated cellulose, a new cellulose product: properties, uses, and commercial potential*, J. Appl. Polym. Sci.: Appl. Polym. Symp.;(United States), ITT Rayonier Inc., Shelton, WA: 1983.
6. Boldizar, A.; Klason, C.; Kubat, J.; Näslund, P.; Saha, P., Prehydrolyzed cellulose as reinforcing filler for thermoplastics. *Int. J. Polymer. Mater.* **1987,** *11* (4), 229-262.
7. Favier, V.; Canova, G.; Cavaillé, J.; Chanzy, H.; Dufresne, A.; Gauthier, C., Nanocomposite materials from latex and cellulose whiskers. *Polym. Adv. Technol.* **1995,** *6* (5), 351-355.
8. Angles, M. N.; Dufresne, A., Plasticized starch/tunicin whiskers nanocomposite materials. 2. Mechanical behavior. *Macromolecules* **2001,** *34* (9), 2921-2931.
9. Martins, I. M.; Magina, S. P.; Oliveira, L.; Freire, C. S.; Silvestre, A. J.; Neto, C. P.; Gandini, A., New biocomposites based on thermoplastic starch and bacterial cellulose. *Compos. Sci. Technol.* **2009,** *69* (13), 2163-2168.

10. Svagan, A. J.; Berglund, L. A.; Jensen, P., Cellulose Nanocomposite Biopolymer Foam - Hierarchical Structure Effects on Energy Absorption. *ACS Appl. Mater. Interfaces* **2011,** *3* (5), 1411-1417.

11. Noishiki, Y.; Nishiyama, Y.; Wada, M.; Kuga, S.; Magoshi, J., Mechanical properties of silk fibroin–microcrystalline cellulose composite films. *J. Appl. Polym. Sci.* **2002,** *86* (13), 3425-3429.

12. Park, D. J.; Choi, Y.; Heo, S.; Cho, S. Y.; Jin, H.-J., Bacterial cellulose nanocrystals-embedded silk nanofibers. *J. Nanosci. Nanotechnol.* **2012,** *12* (7), 6139-6144.

13. de Mesquita, J. P.; Donnici, C. L.; Teixeira, I. F.; Pereira, F. V., Bio-based nanocomposites obtained through covalent linkage between chitosan and cellulose nanocrystals. *Carbohydr. Polym.* **2012,** *90* (1), 210-217.

14. Naseri, N.; Mathew, A. P.; Girandon, L.; Fröhlich, M.; Oksman, K., Porous electrospun nanocomposite mats based on chitosan–cellulose nanocrystals for wound dressing: effect of surface characteristics of nanocrystals. *Cellulose* **2015,** *22* (1), 521-534.

15. Arrieta, M. P.; Fortunati, E.; Dominici, F.; Rayón, E.; López, J.; Kenny, J., Multifunctional PLA–PHB/cellulose nanocrystal films: processing, structural and thermal properties. *Carbohydr. Polym.* **2014,** *107*, 16-24.

16. Chen, J.; Xu, C.; Wu, D.; Pan, K.; Qian, A.; Sha, Y.; Wang, L.; Tong, W., Insights into the nucleation role of cellulose crystals during crystallization of poly (β-hydroxybutyrate). *Carbohydr. Polym.* **2015,** *134*, 508-515.

17. Roohani, M.; Habibi, Y.; Belgacem, N. M.; Ebrahim, G.; Karimi, A. N.; Dufresne, A., Cellulose whiskers reinforced polyvinyl alcohol copolymers nanocomposites. *Eur. Polym. J.* **2008,** *44* (8), 2489-2498.

18. Peresin, M. S.; Habibi, Y.; Zoppe, J. O.; Pawlak, J. J.; Rojas, O. J., Nanofiber composites of polyvinyl alcohol and cellulose nanocrystals: manufacture and characterization. *Biomacromolecules* **2010,** *11* (3), 674-681.

19. Lee, W. J.; Clancy, A. J.; Kontturi, E.; Bismarck, A.; Shaffer, M. S., Strong and stiff: high-performance cellulose nanocrystal/poly (vinyl alcohol) composite fibers. *ACS Appl. Mater. Interfaces* **2016,** *8* (46), 31500-31504.

20. Oksman, K.; Mathew, A. P.; Bondeson, D.; Kvien, I., Manufacturing process of cellulose whiskers/polylactic acid nanocomposites. *Compos. Sci. Technol.* **2006,** *66* (15), 2776-2784.

21. Pei, A.; Zhou, Q.; Berglund, L. A., Functionalized cellulose nanocrystals as biobased nucleation agents in poly (l-lactide)(PLLA)–Crystallization and mechanical property effects. *Compos. Sci. Technol.* **2010,** *70* (5), 815-821.

22. Fortunati, E.; Peltzer, M.; Armentano, I.; Torre, L.; Jiménez, A.; Kenny, J., Effects of modified cellulose nanocrystals on the barrier and migration properties of PLA nano-biocomposites. *Carbohydr. Polym.* **2012,** *90* (2), 948-956.

23. Dhar, P.; Kumar, A.; Katiyar, V., Magnetic cellulose nanocrystal based anisotropic polylactic acid nanocomposite films: influence on electrical, magnetic, thermal, and mechanical properties. *ACS Appl. Mater. Interfaces* **2016,** *8* (28), 18393-18409.

24. Saito, T.; Nishiyama, Y.; Putaux, J.-L.; Vignon, M.; Isogai, A., Homogeneous suspensions of individualized microfibrils from TEMPO-catalyzed oxidation of native cellulose. *Biomacromolecules* **2006,** *7* (6), 1687-1691.

25. Isogai, A.; Saito, T.; Fukuzumi, H., TEMPO-oxidized cellulose nanofibers. *Nanoscale* **2011,** *3* (1), 71-85.

26. Fujisawa, S.; Saito, T.; Kimura, S.; Iwata, T.; Isogai, A., Surface engineering of ultrafine cellulose nanofibrils toward polymer nanocomposite materials. *Biomacromolecules* **2013,** *14* (5), 1541-1546.

27. Endo, R.; Saito, T.; Isogai, A., TEMPO-oxidized cellulose nanofibril/poly (vinyl alcohol) composite drawn fibers. *Polymer* **2013,** *54* (2), 935-941.

28. Fujisawa, S.; Saito, T.; Kimura, S.; Iwata, T.; Isogai, A., Comparison of mechanical reinforcement effects of surface-modified cellulose nanofibrils and carbon nanotubes in PLLA composites. *Compos. Sci. Technol.* **2014,** *90*, 96-101.

29. Fukuzumi, H.; Saito, T.; Iwata, T.; Kumamoto, Y.; Isogai, A., Transparent and high gas barrier films of cellulose nanofibers prepared by TEMPO-mediated oxidation. *Biomacromolecules* **2008,** *10* (1), 162-165.

30. Habibi, Y.; Goffin, A.-L.; Schiltz, N.; Duquesne, E.; Dubois, P.; Dufresne, A., Bionanocomposites based on poly (ε-caprolactone)-grafted cellulose nanocrystals by ring-opening polymerization. *J. Mater. Chem.* **2008,** *18* (41), 5002-5010.

31. Li, Z. Q.; Zhou, X. D.; Pei, C. H., Synthesis of PLA-co-PGMA copolymer and its application in the surface modification of bacterial cellulose. *Int. J. Polymer. Mater.* **2010,** *59* (9), 725-737.

32. Harrisson, S.; Drisko, G. L.; Malmström, E.; Hult, A.; Wooley, K. L., Hybrid rigid/soft and biologic/synthetic materials: polymers grafted onto cellulose microcrystals. *Biomacromolecules* **2011,** *12* (4), 1214-1223.

33. Habibi, Y., Key advances in the chemical modification of nanocelluloses. *Chem. Soc. Rev.* **2014,** *43* (5), 1519-1542.

34. Araki, J.; Wada, M.; Kuga, S., Steric stabilization of a cellulose microcrystal suspension by poly (ethylene glycol) grafting. *Langmuir* **2001,** *17* (1), 21-27.

35. Lasseuguette, E., Grafting onto microfibrils of native cellulose. *Cellulose* **2008,** *15* (4), 571-580.

36. Tang, H.; Butchosa, N.; Zhou, Q., A transparent, hazy, and strong macroscopic ribbon of oriented cellulose nanofibrils bearing poly (ethylene glycol). *Adv. Mater.* **2015,** *27* (12), 2070-2076.

37. Briggs, W. F.; Bullard, E. M. Coextruded thermoplastic stretch-wrap. 4,399,180, 1983.

38. Wang, X.; Bradford, P. D.; Liu, W.; Zhao, H.; Inoue, Y.; Maria, J.-P.; Li, Q.; Yuan, F.-G.; Zhu, Y., Mechanical and electrical property improvement in CNT/Nylon composites through drawing and stretching. *Compos. Sci. Technol.* **2011,** *71* (14), 1677-1683.

39. Nam, T. H.; Goto, K.; Nakayama, H.; Oshima, K.; Premalal, V.; Shimamura, Y.; Inoue, Y.; Naito, K.; Kobayashi, S., Effects of stretching on mechanical properties of aligned multi-walled carbon nanotube/epoxy composites. *Comp. Part A* **2014,** *64*, 194-202.

40. Grijpma, D. W.; Altpeter, H.; Bevis, M. J.; Feijen, J., Improvement of the mechanical properties of poly (D, L‐lactide) by orientation. *Polym. Int.* **2002,** *51* (10), 845-851.

41. Velazquez‐Infante, J. C.; Gamez‐Perez, J.; Franco‐Urquiza, E. A.; Santana, O.; Carrasco, F.; Ll Maspoch, M., Effect of the unidirectional drawing on the thermal and mechanical properties of PLA films with different L‐isomer content. *J. Appl. Polym. Sci.* **2013,** *127* (4), 2661-2669.

42. Mai, F.; Tu, W.; Bilotti, E.; Peijs, T., The influence of solid-state drawing on mechanical properties and hydrolytic degradation of melt-spun poly (lactic acid)(PLA) tapes. *Fibers* **2015,** *3* (4), 523-538.

43. Tabatabaei, S. H.; Ajji, A., Crystal structure and orientation of uniaxially and biaxially oriented PLA and PP nanoclay composite films. *J. Appl. Polym. Sci.* **2012,** *124* (6), 4854-4863.

44. Blaker, J. J.; Lee, K.-Y.; Walters, M.; Drouet, M.; Bismarck, A., Aligned unidirectional PLA/bacterial cellulose nanocomposite fibre reinforced PDLLA composites. *React. Funct. Polym.* **2014,** *85*, 185-192.

45. Mai, F.; Deng, H.; Tu, W.; Chankajorn, S.; Fu, Q.; Bilotti, E.; Peijs, T., Oriented Poly (lactic acid)/Carbon Nanotube Composite Tapes with High Electrical Conductivity and Mechanical Properties. *Macromol. Mater. Eng.* **2015,** *300* (12), 1257-1267.

46. Singh, A. A.; Geng, S.; Herrera, N.; Oksman, K., Aligned plasticized polylactic acid cellulose nanocomposite tapes: Effect of drawing conditions. *Comp. Part A* **2018,** *104*, 101-107.

47. Jonoobi, M.; Mathew, A. P.; Oksman, K., Producing low-cost cellulose nanofiber from sludge as new source of raw materials. *Ind. Crops Prod.* **2012,** *40*, 232-238.

48. Berglund, L.; Noël, M.; Aitomäki, Y.; Öman, T.; Oksman, K., Production potential of cellulose nanofibers from industrial residues: Efficiency and nanofiber characteristics. *Ind. Crops Prod.* **2016,** *92*, 84-92.

49. Tunney, J. J.; Detellier, C., Aluminosilicate Nanocomposite Materials. Poly (ethylene glycol)− Kaolinite Intercalates. *Chem. Mater.* **1996,** *8* (4), 927-935.

50. Wu, J.; Lan, Z.; Lin, J.; Huang, M.; Hao, S.; Sato, T.; Yin, S., A Novel Thermosetting Gel Electrolyte for Stable Quasi‐Solid‐State Dye‐Sensitized Solar Cells. *Adv. Mater.* **2007,** *19* (22), 4006-4011.

51. Saini, S.; Quinot, D.; Lavoine, N.; Belgacem, M. N.; Bras, J., β-Cyclodextrin-grafted TEMPO-oxidized cellulose nanofibers for sustained release of essential oil. *J. Mater. Sci.*, 1-13.

52. Okita, Y.; Saito, T.; Isogai, A., Entire surface oxidation of various cellulose microfibrils by TEMPO-mediated oxidation. *Biomacromolecules* **2010,** *11* (6), 1696-1700.

53. de Gennes, P., Conformations of polymers attached to an interface. *Macromolecules* **1980,** *13* (5), 1069-1075.

54. Wang, Z.; Ciselli, P.; Peijs, T., The extraordinary reinforcing efficiency of single-walled carbon nanotubes in oriented poly (vinyl alcohol) tapes. *Nanotechnology* **2007,** *18* (45), 455709.

55. Brant, D. A.; Tonelli, A. E.; Flory, P. J., The configurational statistics of random poly (lactic acid) chains. II. Theory. *Macromolecules* **1969,** *2* (3), 228-235.

56. Puntel, E.; Deseri, L.; Fried, E., Wrinkling of a stretched thin sheet. *Journal of Elasticity* **2011,** *105* (1), 137-170.

57. Sun, S.-P.; Wei, M.; Olson, J. R.; Shaw, M. T., Alkali etching of a poly (lactide) fiber. *ACS Appl. Mater. Interfaces* **2009,** *1* (7), 1572-1578.

58. Iwamoto, S.; Isogai, A.; Iwata, T., Structure and mechanical properties of wet-spun fibers made from natural cellulose nanofibers. *Biomacromolecules* **2011,** *12* (3), 831-836.

59. Sehaqui, H.; Ezekiel Mushi, N.; Morimune, S.; Salajkova, M.; Nishino, T.; Berglund, L. A., Cellulose nanofiber orientation in nanopaper and nanocomposites by cold drawing. *ACS Appl. Mater. Interfaces* **2012,** *4* (2), 1043-1049.

60. Pahimanolis, N.; Salminen, A.; Penttilä, P. A.; Korhonen, J. T.; Johansson, L.-S.; Ruokolainen, J.; Serimaa, R.; Seppälä, J., Nanofibrillated cellulose/carboxymethyl cellulose composite with improved wet strength. *Cellulose* **2013,** *20* (3), 1459-1468.

61. Wang, J.; Cheng, Q.; Lin, L.; Jiang, L., Synergistic toughening of bioinspired poly (vinyl alcohol)–clay–nanofibrillar cellulose artificial nacre. *ACS Nano* **2014,** *8* (3), 2739-2745.

62. Hamedi, M. M.; Hajian, A.; Fall, A. B.; Håkansson, K.; Salajkova, M.; Lundell, F.; Wågberg, L.; Berglund, L. A., Highly conducting, strong nanocomposites based on nanocellulose-assisted aqueous dispersions of single-wall carbon nanotubes. *ACS Nano* **2014,** *8* (3), 2467-2476.

63. Peng, J.; Ellingham, T.; Sabo, R.; Clemons, C. M.; Turng, L. S., Oriented polyvinyl alcohol films using short cellulose nanofibrils as a reinforcement. *J. Appl. Polym. Sci.* **2015,** *132* (48).

64. Fujisawa, S.; Togawa, E.; Hayashi, N., Orientation control of cellulose nanofibrils in all-cellulose composites and mechanical properties of the films. *J. Wood Sci.* **2016,** *62* (2), 174-180.

65. Lundahl, M. J.; Cunha, A. G.; Rojo, E.; Papageorgiou, A. C.; Rautkari, L.; Arboleda, J. C.; Rojas, O. J., Strength and water interactions of cellulose I filaments wet-spun from cellulose nanofibril hydrogels. *Scientific reports* **2016,** *6*, 30695.

66. Zhu, M.; Wang, Y.; Zhu, S.; Xu, L.; Jia, C.; Dai, J.; Song, J.; Yao, Y.; Wang, Y.; Li, Y., Anisotropic, transparent films with aligned cellulose nanofibers. *Adv. Mater.* **2017,** *29* (21).

67. Wang, S.; Jiang, F.; Xu, X.; Kuang, Y.; Fu, K.; Hitz, E.; Hu, L., Super‐Strong, Super‐Stiff Macrofibers with Aligned, Long Bacterial Cellulose Nanofibers. *Adv. Mater.* **2017,** *29* (35).

68. Mohammadi, P.; Toivonen, M. S.; Ikkala, O.; Wagermaier, W.; Linder, M. B., Aligning cellulose nanofibril dispersions for tougher fibers. *Scientific Reports* **2017,** *7* (1), 11860.

69. Yao, J.; Chen, S.; Chen, Y.; Wang, B.; Pei, Q.; Wang, H., Macrofibers with high mechanical performance based on aligned bacterial cellulose nanofibers. *ACS Appl. Mater. Interfaces* **2017,** *9* (24), 20330-20339.

70. Mittal, N.; Jansson, R.; Widhe, M.; Benselfelt, T.; Håkansson, K. M.; Lundell, F.; Hedhammar, M.; Söderberg, L. D., Ultrastrong and Bioactive Nanostructured Bio-Based Composites. *ACS Nano* **2017,** *11* (5), 5148-5159.

71. Pennings, A. v.; Van der Mark, J.; Kiel, A., Hydrodynamically induced crystallization of polymers from solution. *Kolloid Z. Z. Polym.* **1970,** *237* (2), 336-358.

72. Herrera, N.; Mathew, A. P.; Oksman, K., Plasticized polylactic acid/cellulose nanocomposites prepared using melt-extrusion and liquid feeding: mechanical, thermal and optical properties. *Compos. Sci. Technol.* **2015,** *106*, 149-155.

73. Lizundia, E.; Larrañaga, A.; Vilas, J. L.; León, L. M., Three-dimensional orientation of poly (L-lactide) crystals under uniaxial drawing. *RSC Advances* **2016,** *6* (15), 11943-11951.

74. Hu, L.; Zheng, G.; Yao, J.; Liu, N.; Weil, B.; Eskilsson, M.; Karabulut, E.; Ruan, Z.; Fan, S.; Bloking, J. T., Transparent and conductive paper from nanocellulose fibers. *Energy & Environmental Science* **2013,** *6* (2), 513-518.

75. Zhu, M.; Song, J.; Li, T.; Gong, A.; Wang, Y.; Dai, J.; Yao, Y.; Luo, W.; Henderson, D.; Hu, L., Highly anisotropic, highly transparent wood composites. *Adv. Mater.* **2016,** *28* (26), 5181-5187.

For Table of Contents Use

High-strength, High-toughness Aligned Polymer-based Nanocomposite Reinforced with Ultra-low Weight Fraction of Functionalized Nanocellulose

Shiyu Geng,[1,3] *Kun Yao,*[2,3] *Qi Zhou*[2,3] *and Kristiina Oksman*[1,4]*

[1]Division of Materials Science, Department of Engineering Sciences and Mathematics, Luleå University of Technology, SE-971 87, Luleå, Sweden

[2]Division of Glycoscience, Department of Chemistry, KTH Royal Institute of Technology, AlbaNova University Centre, SE-106 91, Stockholm, Sweden

[3]Wallenberg Wood Science Center, Department of Fiber and Polymer Technology, KTH Royal Institute of Technology, SE-100 44 Stockholm, Sweden

[4]Fibre and Particle Engineering, University of Oulu, FI-90014, Oulu, Finland